Water Science & Technology

Water Science & Technology Vol 87 No 3, 729 doi: 10.2166/wst.2023.012

Promising antibacterial activities of anethole and green-synthesized magnetite nanoparticles against multiple antibiotic-resistant bacteria

Marwa E. El-Sesy [a,*] and Sahar A. Othman[b]

[a] Microbiology Department, Central Laboratory for Environmental Quality Monitoring (CLEQM), National Water Research Center (NWRC), Cairo, Egypt
[b] Inorganic Chemistry Department, Central Laboratory for Environmental Quality Monitoring (CLEQM), National Water Research Center (NWRC), Cairo, Egypt
*Corresponding author. E-mail: marwa.micro@gmail.com; marwa_elsesy@nwrc.gov.eg

ME-S, 0000-0002-9984-9383

ABSTRACT

The emergence of antibiotic resistance is considered a major threat, and this problem is exacerbated due to the excessive use of antibiotics. Therefore, it is necessary to find new antimicrobials that are effective against pathogenic bacteria resistant to existing antimicrobials. This study presents a novel antimicrobial approach for the bio-control of multi-antibiotic-resistant (MAR) bacteria. Ten antibiotic discs were used to evaluate the bacterial sensitivity. Five bacterial strains showed resistance to all the tested antibiotic groups. The following MAR bacterial strains were selected, and their identification was confirmed by 16S rRNA with an accession number on the NCBI: *Shigella flexneri* MZ350855.1; *Klebsiella aerogenes* MZ352107.1; *Serratia marcescens* MZ618709.1; *Yersinia enterocolitica* MZ673567.1; and *Achromobacter denitrificans* OK560350.1. Star anise extract (SAE) gives the highest inhibitory efficiency against isolated MAR bacteria between three local plant extracts. SAE was used to synthesize magnetite nanoparticles (MNPs) using a simple and eco-friendly green biosynthesis technique. Synthesized MNPs were characterized by X-ray diffraction, ultraviolet–visible spectroscopy, Fourier transform infrared, and transmission electron microscopy techniques. The effect of synthesized magnetic nanoparticles for wastewater treatment in bacterial portion demonstrated remarkable bactericidal performance against total bacterial count with a percentage reduction of 84% using 0.05 g, and the efficiency of decreasing heavy metals was estimated.

Key words: anethole, antibacterial activities, magnetite nanoparticles, multidrug-resistant bacteria, star anise

HIGHLIGHTS

- Elucidate the antibacterial properties of three plant crude water extracts against different multi-antibiotic-resistant (MAR) isolated bacteria.
- The green synthetic approaches for MNPs using SAE as an alternative source to the conventional chemical method.
- Using this technique as an approach for wastewater treatment.

GRAPHICAL ABSTRACT

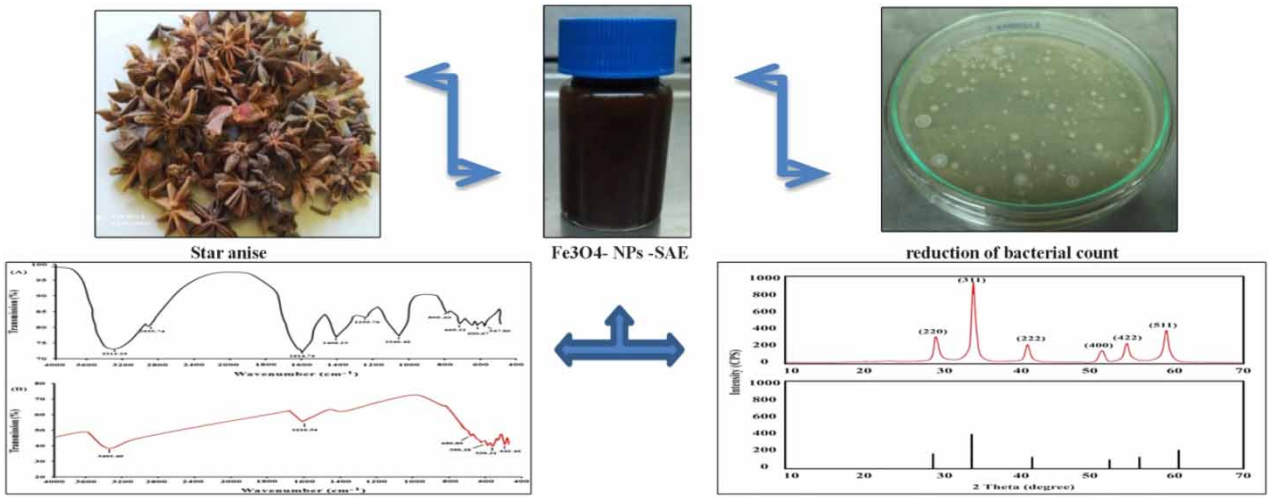

1. INTRODUCTION

Patients receiving antibiotic therapy harbor a large number of antibiotic-resistant bacteria in their intestinal tracts, where they are excreted in large numbers in feces and eventually can contaminate the aquatic environment through fecal materials. Consequently, multi-antibiotic-resistant (MAR) bacteria have been detected in raw sewage, rivers, and other polluted environments (Kessie *et al.* 1998).

MAR microorganisms (i.e., viruses, bacteria, and fungi) are resistant to multiple antimicrobial agents, making it extremely difficult for healthcare workers to treat patients and ultimately resulting in increased morbidity and mortality rates (Santos *et al.* 2013). MAR is a significant issue whose effects on public health and socioeconomic sectors are imminent. MAR bacteria are expected to be responsible for the death of many people. The resistance spectrum varies considerably from region to region (World Health Organization 2014). MAR bacteria pose a significant problem in high-income countries, while these data are unavailable for African countries (Tadesse *et al.* 2017).

Returning to nature has endowed us with vast botanical wealth. Some natural plants have been a source of novel natural bioactive compounds for a very long time, including natural microbial inhibitors and new biologically active compounds that can be used directly as antibacterial compounds; these compounds can be used to treat MAR bacteria. The significance of natural plant extracts is due to their low toxicity, economic viability, and eco-friendliness (Kloy *et al.* 2020), and they represent one of the alternative methods in wastewater treatment and render it suitable for human consumption.

In an attempt to discover new antimicrobial agents, many studies and surveys have been carried out worldwide on many plants according to the plant flora of a respective region (Sarg *et al.* 1990). According to Muralikrishna *et al.* (2014), aloe vera (AV) is a succulent plant species used in herbal medicine since the beginning of the first century. Aloe vera extracts (AVEs) are widely used as an alternative medicine. Previous studies reported that star anise extract (SAE; *Illicium verum*) was assessed for antimicrobial activity against 25 different genera of bacteria, including animal and plant pathogens, food, and spoilage bacteria. Results showed that the SAE inhibited the growth of 81.1% of the test organisms (Dorman & Deans 2000; Aly *et al.* 2016). This plant received significant attention after shikimic acid was extracted from star anise, which was used to manufacture Tamiflu, which was used as a drug to treat influenza (Wang *et al.* 2011). A study was conducted to evaluate using the extracts of rosemary (*Rosmarinus officinalis*) in folk medicine, which were screened for their activity *in vitro* against some Gram-positive and Gram-negative pathogenic bacteria (César de Souza Vasconcelos *et al.* 2003). Several studies reported that fresh and dried rosemary leaves have many potential effects, including antibacterial, antifungal, antiviral, and other activities (Devatkal *et al.* 2013; Houston *et al.* 2017).

Nanomolecules represent an alternative to conventional antimicrobial agents, where many researchers reported the ability to use some metal nanoparticles for wastewater treatment problems. Due to their large surface-to-volume ratio, they retain potent antibacterial properties (Klnight *et al.* 2003; Savage & Diallo 2005). In addition to its antimicrobial applications for water disinfection, it has a significant effect on the adsorption of various heavy metals such as Pb^{2+}, Cd^{2+}, Cu^{2+}, and

Ni^{2+} (Giraldo *et al.* 2013). Nanomolecules may be made using polymers, lipids, and metals (Kim *et al.* 2012). Nanoparticles are nano-sized molecules (less than 100 nm in diameter) with a large surface area compared to volume ratio, allowing them to penetrate bacterial cells relatively easily (Chen *et al.* 2012). Nanoparticles can be attached to microbial surfaces and cause a decrease in both cell mobility and nutrient flow. Different sizes and shapes of nanomaterials can be exploited for developing nanocomposites with antimicrobial activity (Pinto *et al.* 2012).

Chemical, physical, and biological methods can be used to synthesize magnetite nanoparticles (MNPs). The chemical reduction method is used, as it is a simple, quick, and inexpensive method. Using reducing agents in the synthesis of MNPs by a chemical reduction method may result in a toxic effect and a lack of environmental friendliness (Demchenko *et al.* 2020). Consequently, the reducing agent derived from plants may become one of the alternative options due to its lower toxicity and environmental friendliness. Bioreductors from plants can be obtained since their secondary metabolites, such as flavonoids, saponins, tannins, and terpenoids give antioxidant activity (Handayani *et al.* 2020).

There are successful studies in synthesizing MNPs using plant extracts (Sri *et al.* 2015). For instance, the fruit extract of *Artemisia annua* (Basavegowda *et al.* 2014a), the leaf extract of *Perilla frutescens* (Basavegowda *et al.* 2014a), *Tridax procumbens* (Senthil & Ramesh 2012), peel extract of plantain (Venkateswarlu *et al.* 2013), and also seed extract of grape proanthocyanidin (Narayanan *et al.* 2012). Based on several review studies, no specific research was done on magnetite synthesis by star anise, and this motivates us to synthesize this. Hence, this research proposes a novel green technique for synthesizing Fe_3O_4–NPs using star anise.

Concerning the above scope, the present study aims to investigate (i) the antibacterial activity of the crude water extract of three plants against the isolated MAR bacteria, (ii) the green synthetic approaches for MNPs using star anise water extract, which is an alternative source to the conventional chemical method, (iii) further application of synthesized magnetite by star anise in wastewater treatment with determining the antibacterial activity as well as efficiency in trace metal removal.

2. MATERIALS AND METHODS

2.1. Sampling, isolation, and purification of bacterial isolates

The outlet points of three different drain resources have been selected to carry out the study. Agricultural drainage water from Sahl El-Husseiniya drain, Sharqia Governorate; industrial wastewater from Al-Khadrawiya drain, Menufia Governorate; and sewage-contaminated water from Bahr El-Baqr drains, Port Saied Governorate were collected according to the standard methods for the examination of water and wastewater (APHA 2017).

Bacterial strains from each water resource were isolated from the total viable bacterial count plates throughout the study. Growing colonies of each plate were differentiated and categorized according to the cultural characteristics, then purified and maintained for further identification.

2.2. Antibiotic sensitivity test for bacterial isolates

According to the Clinical and Laboratory Standards Institute (2019), the susceptibility behavior of the purified bacterial isolates from the wastewater samples to the antibiotics was determined on Mueller–Hinton agar by the disc diffusion method using 10 commercially available antibiotic discs belonging to eight different antibiotic groups, and discs were obtained from Pasteur lab and Oxoid. The following antibiotic discs were used: amoxicillin/clavulanate AG (30 μg); ampicillin AM (10 μg); vancomycin VA (30 μg); neomycin N (30 μg); tetracycline TE (30 μg); clindamycin DA (30 μg); erythromycin E (10 μg); cefotaxime CTX (15 μg); cefepime C (10 μg); and ofloxacin OFX (30 μg). Control Mueller–Hinton agar plates were incubated without antibiotic discs. Inhibition zone diameters (IZDs) were measured in millimeters (mm) (Bauer 1966). When a microorganism becomes resistant to more than one antimicrobial medication in three or more antimicrobial classes, MAR occurs (Sawatzky *et al.* 2015). The results were categorized as R (resistant), I (intermediate sensitive), and S (sensitive).

2.3. Identification of most MAR bacterial isolates

The selected purified isolate MAR bacteria exhibiting acquired antibiotic resistance patterns were identified utilizing culture characteristics, Gram's stain, and biochemical characterization as described by Holt & Krieg (1984) and Sneath (1986).

Finally, the pre-identified isolates were confirmed by the genetic analysis of 16S rRNA. Bacterial DNA was extracted and purified using the protocol of Gene Jet Genomic DNA Purification Kit (K0721; Thermo Fisher Scientific) and then used as a template to amplify the 16S rDNA gene by polymerase chain reaction (PCR). The 16S gene was amplified using universal forward primer 27F of (5′-AGA GTT TGA TCC TGG CTC AG-3′) and 1492R (5′-CGG YTA CCT TGT TAC GAC TT-3′)

was used to amplify the 16S gene. The PCR cycles were run as follows: initial denaturation for 5 min at 94 °C, denaturation for 1 min at 94 °C, annealing for 1 min at 55 °C and extension for 2 min at 72 °C, and the final extension for another 1 mL of first and 10 min at 72 °C. The previous cycles were repeated 30 times. The amplification products were sequenced utilizing Biomolecular Research Services (GATC Biotech, Konstanz, Germany) using ABI (Applied Bio systems) 3730 X DNA sequencer (Hitachi) with the same primers. The 16S rRNA gene sequences obtained were aligned to the NCBI Gen Bank database through BLAST analysis with the maximum similarity and identity using gene alignment database (http://blast.ncbi.nlm.nih.gov/Blast.cgi), sequences were aligned with the CLUSTAL W program and analyzed with the MEGA-X software. The phylogenic tree was carried out using the Maximum Likelihood method with bootstrap values calculated from 1,000 replicate runs (Megha *et al.* 2015).

2.4. Chemicals, reagents, and materials

The plants used in this study were purchased from the local market in Cairo, Egypt, and their inhibitory effect against MAR bacteria was examined. All chemicals used in this experiment were received from Al-Gomhorya Company for chemicals, Egypt. Materials used in the synthesis process were of analytical grade.

2.5. Preparation of crude plant extract against bacterial isolates

Star anise (*I. verum*) fruit, aloe vera (AV) leaves, and rosemary (*R. officinalis*) leaves extracts were studied for their inhibitory activity against MAR bacteria.

In order to prepare SAE, dried fruits were ground to a fine powder and stored. Rosemary and AV leaves were cleaned for extract preparation. After drying in shade at room temperature and then subjected to oven drying at 40 °C, the particles were crushed into smaller dimensions and then pulverized using a sterile mortar (Moulinex). The plant powders were kept in a sterile, airtight plastic container in the refrigerator. Twenty grams (20 g) of the ground plant samples were soaked in 100 mL of sterilized water then allowed to stand for about 72 h for extraction. After 72 h, the supernatant was collected and filtered using Whatman filter paper No. 1. The filtered samples were sterilized and filtered again by a 0.22 μm Millipore membrane filter (Whatman, Kent, UK). The filtrate was then stored in Eppendorf tubes at a temperature of −4 °C until the assessment of its inhibitory effect (Etemadifar *et al.* 2018).

The agar disc diffusion technique was utilized to determine the antibacterial activity of the crude plant extract against the selected MAR bacteria (Clinical and Laboratory Standards Institute 2019). The bacterial suspension was spread on a solid plate using a sterile swab aseptically and allowed to dry. Sterile filter paper discs (Whatman no. 5, 6 mm in diameter) were loaded with the plant extract at a concentration of 10 mg/disc; the discs were then placed on top of the seeded medium and gently pressed to ensure contact. The plates were incubated at 37 °C overnight. After the incubation period, inhibition zones on the medium were measured in millimeters. All the experiments were performed three independent times (Figure 1).

Figure 1 | Photographs of three different plant extracts: (a) star anise (*Illicium verum*) fruit, (b) aloe vera leaves, and (c) rosemary (*Rosmarinus officinalis*) leaves.

2.6. Statistical analysis

Each test was conducted in triplicate. The mean and standard deviation (SD) of the growth inhibition zone diameter in the agar disk diffusion method of the extracts were determined. Data were analyzed using Statistical Package for Social Sciences for Windows, version 19.0 (SPSS Inc.).

2.7. Purification and identification of the active component of star anise

Analytical thin layer chromatography (TLC) was carried out to purify the active components of star anise fruit extract (SAE), where TLC was placed in contact with the bacterial culture. For the separation of star anise constituents, first, leaving approximately 1 cm on the sides of the TLC plate (20 cm × 20 cm, 0.21 mm thickness, Whatman cellulose chromatography paper), which was marked with a pencil, and the prepared SAE was spotted on the marked line. About 5 μL of 10 mg/mL concentration of tested SAE was spotted with a band length of 10 mm chromatographic Whatman cellulose chromatography paper, and then allowed to dry for a few minutes. Afterward, the plate was developed with a running solvent system of ethyl acetate, methanol, and formic acid in a ratio (of 2:1:0.5 v/v). The paper was placed in an airtight chromatographic chamber saturated with the solvent mixture. Spots were separated by running on the TLC plate in the selected solvent system. Before the solvent reached the maximum point, the plate was removed. The retention factor (Rf) values of separated compounds were determined to quantify the distance each component of a mixture travels. Rf value is defined as the ratio of the spot's displacement above the baseline to the solvent front's displacement above the origin (Prakash *et al.* 2014). Bio-autography of different Rf values against tested MDR bacteria was performed using the agar well diffusion method when the plate was completely dry.

2.8. Gas chromatography–mass spectrometry analysis

Bioactive compounds of SAE extracted by TLC were analyzed by gas chromatography–mass spectrometry (GC–MS) using a TRACE GC Ultra Gas Chromatograph (Thermo Fisher Scientific Corp.) equipped with a thermo mass spectrometer detector (ISQ Single Qua drupole Mass Spectrometer). During analysis, an HP5MS UI (crosslinked 5% methyl phenyl Silox) capillary column was utilized (Moniruzzaman *et al.* 2015).

2.9. Biosynthesis and antibacterial activity of MNPs from star anise

Magnetite biosynthesis was carried out utilizing star anise fruit extract; Fe_3O_4–NPs were prepared to utilize the precursor salts ferrous sulfate ($FeSO_4{\cdot}7H_2O$) and ferric chloride ($FeCl_3$) at 1:2 M ratios as follows. Iron (II) sulfate and iron (III) chloride solutions were prepared by dissolving 3.73368 and 4.35695 g of the salts, respectively, in 500 mL of distilled water supplemented with nitrogen gas purging. Nitrogen gas was selected for purging because it is inert to solutions and readily available. After the complete dissolution (transparent solutions) of the salts, the two solutions were mixed and heated at 80 °C using a magnetic stirrer and under atmospheric pressure. After 10 min, different concentrations (2.5, 5, and 10%) of SAE were added to the reaction separately, named SAE1, SAE2 and SAE3 sequentially. After 5 min, 5% NaOH solution was added to the mixture dropwise with a rate of 5 mL min^{-1} to allow the magnetite precipitation uniformly. Once NaOH was added, the reddish-brown color of the mixture changed to brownish-black suspended particles, until complete precipitation of the black precipitate of Fe_3O_4 was achieved (the complete precipitation is indicated by testing the filtrate solution against drops of NaOH.

A conical flask containing 50 mL of 0.01 M Fe_3O_4 was prepared as a negative control (Fauzi *et al.* 2021) and testing the selected MAR bacteria against biosynthesis MNPs using the Kirby–Bauer disc-diffusion method (Clinical and Laboratory Standards Institute 2019). Changes in the color of the reaction mixtures were observed to determine nanoparticle formation characterized by a dark brown color (Figure 2).

2.10. Characterization techniques of MNPs

Further confirmation of synthesis MNPs was checked first using UV – a visible spectrum (Hitachi U-2910 Spectrophotometer (Tokyo, Japan). UV–Vis spectroscopic analysis measurements were performed via continuous scanning in the range of 200–800 nm.

The phase evaluation of the synthesized MNPs solution was performed using an X-ray diffractometer (Rotoflux, Model 10.61, Germany) with Ni-filtered Cu-Kα radiation (0.15406 Å). The voltage and current of X-ray tubes were 30 kV and 20 mA at room temperature of about 25 °C with a step size of 0.05 and diffraction range of $2\theta = 10°–70°$. The diffraction pattern of MNPs was compared with the reference data from the standards compiled by the Joint Committee on Powder

Figure 2 | Photograph showing green-synthesized magnetite nanoparticles (SAE–Fe_3O_4–NPs).

Diffraction and Standards (JCPDS), which involved card No. 04-0829 for MNPs. According to Priyadarsini *et al.* (2020). Purification and concentration of MNPs from the final reaction mixture were assessed using Scherer's Equation ($D = 0.9\lambda/\beta \cos\theta$) to determine the size of the nanoparticles, where D is the nano-size, λ is the wavelength of X-ray, θ is the diffraction angle, and β is full width at half maximum of the peak (Dipankar & Murugan 2012).

Fourier transformer infrared spectroscopy (FTIR) analysis was carried out using Pelkin-Elmer FTIR 1650 spectrophotometer. Finally, the morphological characteristic of MNPS was examined via scanning electron microscope (SEM, JSM 8404, JEOL Limited, Japan) at a 10 kV with magnifications n of 50,000× and 100,000×. The size particle and morphology of samples were inspected in a transmission electron microscope using (TEM, JEM 2100Plus, JEOL Limited, Japan) which was performed at 100 kV.

2.11. Application of green-synthesized MNPs for wastewater treatment

A clean, pre-sterilized container was utilized for the collection of wastewater samples from the Al-Khadrawiya drain, Menufia Governorate (APHA 2017) and directly transported to Central Laboratory for Environmental Quality Monitoring (CLEQM). Five conical flasks were prepared, each containing 1,000 mL of the collected wastewater sample, then treated separately with different amounts of the tested concentration of biosynthesized MNPs (Fe_3O_4–NPs) by SAE (0.05, 0.04, 0.03, 0.02 and 0.01 g), along with a blank experiment, and were shaken for 30 min. The antibacterial effect of synthesized MNPs was examined using the colony forming unit (CFU) detection method where from the stirred solutions, 100 µL of the mixture was spread on nutrient agar plates and then incubated at 37 °C for 24 h, and the number of CFU/mL was counted. The percentage reduction of the bacterial count was calculated using Equation (1).

$$\text{Percentage reduction of bacterial count} = 100 \times \frac{\text{initial CFU} - \text{final CFU}}{\text{Initial CFU}} \quad (1)$$

The inductively coupled plasma (ICP-OES) with ultra sonic nebulizer (USN), Perkin-Elmer Optima 5300, USA, was used for estimating trace metals in the collected control sample and also the treated conical flasks with the examined above concentrations of synthesized nanoparticles in an attempt to investigate the ability of synthesized SAE–Fe_3O_4–NPs in absorption of the metal ions.

3. RESULTS AND DISCUSSION

3.1. Antibiotic susceptibility patterns

About 50 bacterial isolates were isolated from the collected wastewater samples from the three selected locations. Ten antibiotics were used to evaluate the antibiotic susceptibility of the bacterial isolates. The resistance profile of these isolates is presented in Table 1, revealing multiple antibiotic resistances among bacterial isolates. Resistance was mainly directed to ampicillin, erythromycin, and cefepime, where all bacterial isolates (100%) were resistant, while the most active antibiotics were ofloxacin, and about (80%) of bacterial isolates were sensitive, followed by cefotaxime (72%), neomycin (64%), vancomycin (54%), amoxicillin/clavulanate (40%), and clindamycin (32%), and tetracycline (20%). Five of the most resistant bacterial isolates reported in our study were resistant to all groups of antibiotics discs with code no (4, 18, 22, 39, and 47).

Table 1 | Comparative susceptibility of bacterial isolates against different antibiotics

Group & scientific name of antibiotic	Trade name	Antibiotic code	Disc potency (μg/disc)	Resistant bacterial isolate number	Category	Sensitive		Resistant	
						No	%	No	%
1. *Penicillins* Amoxicillin/ Clavulanate	Augmentin	AG	30	1, 4, 6, (8–19), (21–27), 30, 33, 37, 39, 42, 44, 47, 50.	S	20	40	30	60
ampicillin	Ampicillin	AM	10	(1–50)	R	0	100	50	0
2. *Quinolones* ofloxacin	Tarivid	OFX	10	4, 14, 18, 22, 35, 39, 40, 44, 47,49	R	40	80	10	20
3. *Tetracyclines* Tetracycline	Tetracycline	TE	30	(1–23), (29–44), 47	S	10	20	40	80
4. *Aminoglycosides* Neomycin	Neo-rx	**N**	30	(1–7), 10, 18, 22, 28, 30, 31, 39, 40, 44, 46, 47.	I	32	64	18	36
5. *Lincosamides* Clindamycin	lincocin	DA	30	(1–9), (14–19), 23, 24, (29–35), 37, 38, (40–44), 47, 49, 50.	S	16	32	34	68
6. *Macrolides* Erythromycin	Erythromycin	E	10	(1–50)	R	0	100	50	0
7. *Cephalosporins* cefotaxime	Claforan	CTX	30	4, 10, (17–22), 24, 27, 39, 42, 45, 47.	I	36	72	14	28
Cefepime	Maxipime	C	30	(1–50)	R	0	100	50	0
8. *Glycopeptides* Vancomycin	Vancocin	VA	30	(1–5), (10–13), (17–29), 32, 35, 39, 40, 47, 49.	I	27	54	23	46

MAR, multi-antibiotic-resistant.

This finding demonstrates that these isolates are preliminarily to be MAR bacteria, so they were chosen for further studies. The increasing prevalence of MAR bacteria represents global health challenges (World Health Organization 2014). In this respect, Iversen *et al.* (2004) indicated a potential transmission route for pathogenic bacteria from patients in hospitals to hospital sewage, further to surface water, and possibly back to humans. Based on our findings, it was evident that water pollution may play a significant role in the dissemination of hazardous antibiotic-resistant bacteria. The morphological, physiological, and biochemical identification of the MAR bacteria was evaluated according to identification protocols. The sequences of MAR bacterial strains obtained were aligned to the BLAST analysis with the NCBI GenBank database and were identified under accession numbers *Shigella flexneri* MZ350855.1, *Yersinia enterocolitica* MZ673567.1, *Klebsiella aerogenes* MZ352107.1, *Achromobacter denitrificans* OK560350.1, and *Serratia marcescens* MZ618709.1 (Figure 3).

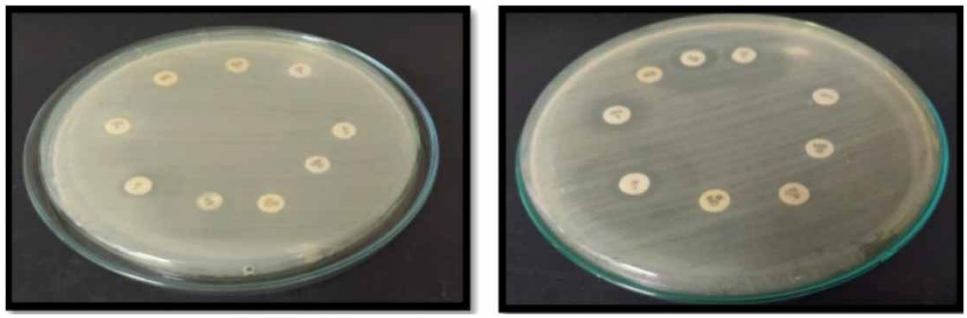

Figure 3 | MAR bacterial strains.

3.2. Antibacterial activity of plant extracts

The antibacterial activity of some medicinal plants is higher than that of some antibiotics, where their bioactive components give them this potency. In our study, the inhibitory effect of three plants against MAR bacteria isolated from collected polluted water samples was proposed. The data of star anise fruit extracts (P1), AV leaves (P2), and rosemary (*R. officinalis*) leaves extracts (P3) are depicted in Table 2 and Figures 4 and 5. Star anise fruit extracts (SAE) produced the highest inhibitory activity against all selected bacteria, reaching 11–17 mm, followed by Rosemary leaves extract, with (4–10 mm). In contrast, AV did not affect MAR bacteria, as shown in Table 2. SAE was selected for purification by TLC and then analyzed by GC–MS as it gives the most and strongest inhibitory activity between the examined extracts against all the MAR-tested bacteria. The

Table 2 | Antibacterial activities of SAEs against MAR bacteria

		IZDs (mm) of bacterial isolates				
		Isolates codes				
Plant codes	**Plant extract**	**4**	**22**	**18**	**39**	**47**
P1	Star anise fruit	12	11	13	16	17
P2	Aloe vera leaf	0	0	0	0	0
P3	Rosemary leaves	5	8	0	10	4

IZDs, inhibition zone diameters.

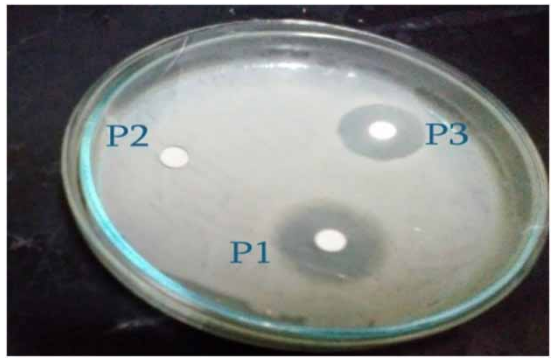

Figure 4 | Antibacterial activities of different plant extracts against MAR bacteria.

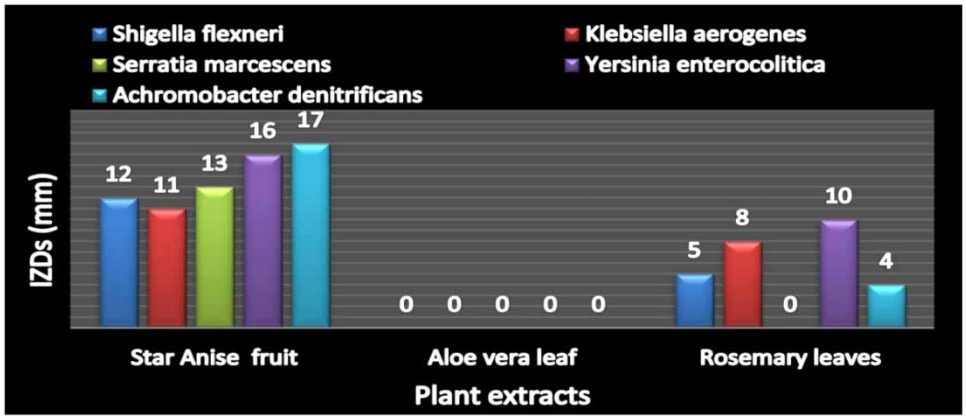

Figure 5 | Antibacterial activity of plant extracts against multidrug-resistant bacteria.

antimicrobial activity of SAE is attributed to the presence of a phenyl group which can damage proteins, so interacting in the cell membrane of the bacteria with the lipids lead to the death of bacterial cell by changing the permeability of the cell membrane (Qiao *et al.* 2018). Consistent with our results with Ismail *et al.* (2012), who reported that only three extracts (star anise, garlic juice, and clove) out of 12 plant extracts were tested for their inhibitory effect versus eight microbial strains showed a high antimicrobial effect against the bacteria under study.

3.3. Identification of MAR bacteria

Using 16S rRNA gene sequencing for the identification of the most resistant bacteria during the study against different antibiotics were submitted to GenBank at the NCBI website under an accession number as follow: *S. flexneri* MZ350855.1; *K. aerogenes* MZ352107.1; *S. marcescens* MZ618709.1; *Y. enterocolitica* MZ673567.1; and *A. denitrificans* OK560350.1 Figure 6 demonstrates the phylogenetic tree of the isolated MAR and others from the NCBI.

3.4. GC–MS analysis

On the TLC chromatogram, the preliminary partial purification of SAE by TLC autobiography revealed positive bands (Table 3). In the TLC assay, the results revealed a clear zone indicating the presence of antibacterial components against the MAR bacterial strains tested, with an Rf value of (0.909) in the TLC assay, compatible with Najdoska *et al.* (2010).

Figure 6 | Phylogenic tree of the MAR bacteria during the study with others from the NCBI.

Table 3 | Antibacterial activity of SAE at different Rf values against the tested bacteria

Bacterial isolates	Solvent *v/v*	Rf	IZDs (mm) of bacterial isolates
Shigella flexneri MZ350855	Ethyl acetate:methanol:formic acid (2:1:0.5)	0.2 0.9	10 12
Klebsiella aerogenes MZ352107		0.7 0.9	10 15
Serratia marcescens MZ618709		0.8 0.9	11 17
Yersinia enterocolitica MZ673567		0.9	13
Achromobacter denitrificans OK560350		0.9	14

Therefore, instrument GC–MS was used for detecting the bioactive compound of SAE, which was found in (0.909) Rf value by TLC (Figure 7).

The mass spectrum of 148 mz was obtained by GC–MS for trans-1-methoxy-4-[prop-1-enil] benzene (anethole), and the results of GC–MS represent that anethole is the primary compound in the star anise (*I. verum*) extract, approximately 98%, which is consistent with the results of (Marquez *et al.* 2008). Trans-1-methoxy-4-[prop-1-enil] benzene (anethole) with formula $C_{10}H_{12}O$ is present as a major significant component that occurs widely in many natural plants, such as star anise (*I. verum*) (Ize-Ludlow *et al.* 2004). Natural anethole occurs in high concentrations in star anise (over 90%), according to Marinov & Valcheva (2015) (Figure 8).

3.5. Green biosynthesis of MNPs from SAE

MNPs were successfully synthesized by using the fruit star anise, as presented in Figure 1. The synthesized MNPs showed a dark black color in the aqueous solution and this is due to the collective oscillation of free electrons present in the reduced MNPs, according to Noginov *et al.* (2007). After adding ferric chloride solution to the plant extract containing the phenolic and flavonoid compounds used as alternative reducing agents (Rengga *et al.* 2017), the nanoparticles may be stabilized by the reduction of Fe^{3+} to Fe^{2+}, as reported by Sonibare *et al.* (2017). The magnetic response of MNPs synthesized using star anise plant extract was confirmed by their migration in a few minutes toward a 0.5 T magnet placed in the proximity of the solution. This result indicates that MNPs with ferromagnetic properties were successfully synthesized and may contribute to cell separation.

3.6. UV–vis spectral analysis

UV–vis spectroscopy was first used to confirm the formation and stability of MNPs in an aqueous colloidal solution with different wavelengths ranging from 200 to 600 nm. The biosynthesized MNPs revealed a high peak at 250 nm (Figure 9). These results are in accordance with those recorded by Njagi *et al.* (2011), who have reported a similar absorbance peak for iron oxide magnetic nanoparticles synthesized using an aqueous sorghum bran extract leaf ranged from 240 to

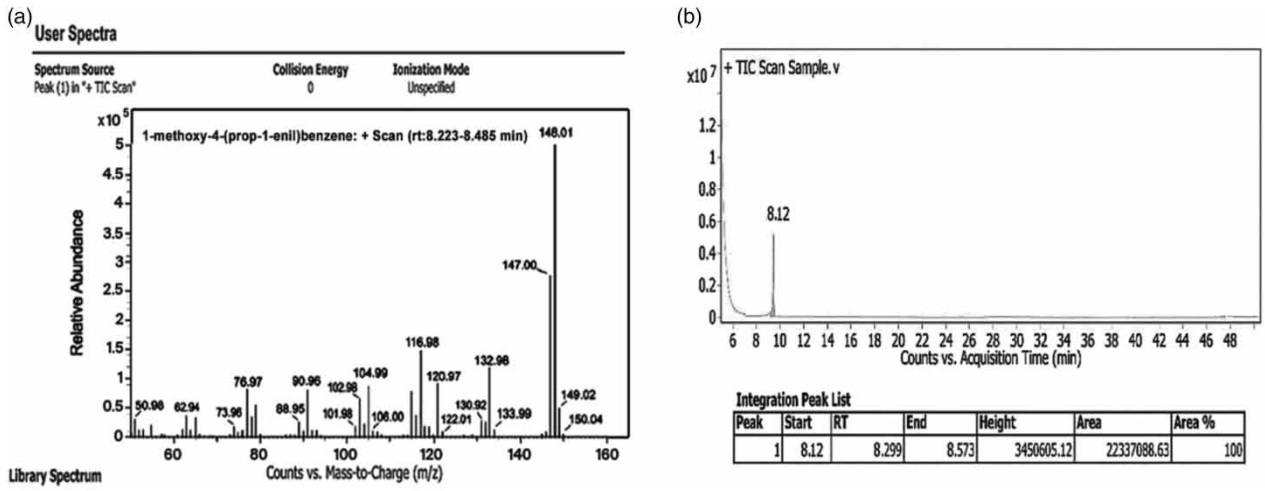

Figure 7 | (a) Gas chromatography–mass spectrometry analysis of (trans-1-methoxy-4-[prop-1-enil] benzene). (b) Thin-layer chromatography (TLC) scan of SAE extract at Rf = 0.9.

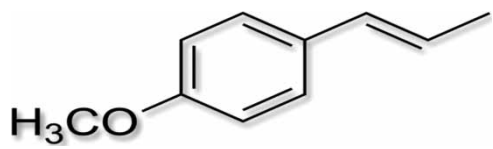

Figure 8 | Chemical structure of trans-1-methoxy-4-[prop-1-enil] benzene (anethole) has the formula of $C_{10}H_{12}O$ (molecular weight: 148.205).

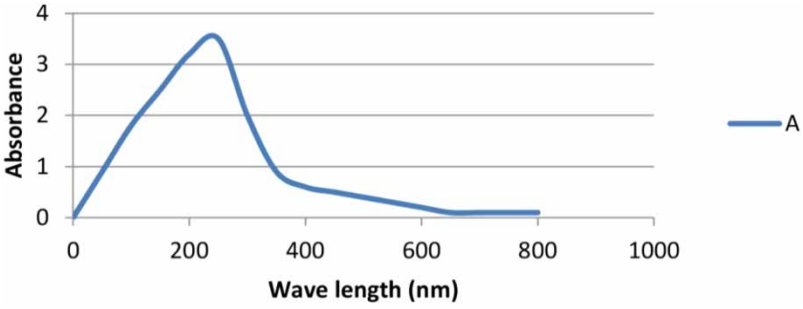

Figure 9 | UV/Vis absorption spectra of the bio-MNPs produced using the SAE.

360 nm. Based on UV–vis results, star anise fruit extract reduced Fe^{3+} to MNPs, and this finding was investigated further to confirm the star anise MNPs synthesis.

3.7. Structural features of magnetic nanoparticles

3.7.1. XRD analysis

Figure 10(a) demonstrates the XRD patterns of synthesized MNPs using the extract of star anise, which was confirmed and proved via the characteristic peaks that appeared in the XRD spectrum. Six different peaks were virtually specified at scattering angles (2θ) of 30.22, 35.60, 45.60, 54.10, 57.68, and 63.10, corresponding to the hkl planes of (220), (311), (222), (400), (422) and (511), respectively. Readily, the diffraction peaks can be indexed to the pure cubic phase of magnetite according to comparison with the standard data from (Joint Committee on Powder Diffraction Standards, JCPDS file, PDF No. 19–0629) according to Basavegowda *et al.* (2014b). In addition, the absence of XRD-detectable impurities confirms that the prepared MNPs have a well-formed crystalline structure and high purity. Consequently, these diffraction peaks reveal the typical crystallite size of the particles.

The particle size of MNPs (SAE–Fe_3O_4–NPs) was estimated using Scherrer's formula from the following Equation (2):

$$D = \frac{k\lambda}{\beta \cos\theta} \tag{2}$$

where D is the nanoparticle size, k is the Scherrer constant which is 0.9 for magnetite; λ is the wavelength of radiation source Cu-kα (0.154056 nm), θ represents the diffraction angel, where β represents the full width at half maximum of the peak (FWHM) (Dipankar & Murugan 2012; Mahdavi *et al.* 2013). By applying the Scherrer equation, the average calculated crystallite sizes of the Fe_3O_4–NPs are in the range of 21–32 nm (Table 4).

3.7.2. Scanning and transmission electron microscopy

In order to evaluate the morphology and uniformity of the synthesized Fe_3O_4-MNPs by star anise plant extract, SEM analysis was performed, and the results are depicted in Figure 10(b). Additionally, the SEM image indicated that the morphology of synthesized SAE–Fe_3O_4–NPs appeared as roughly irregular spherical that aggregated in three-dimensional shape with relatively crystalline in their structure, and that the average particle size of the resultant nanoparticles was between 18 and 33 nm revealed that the resultant nanoparticles particles size was in the range of 18–33 nm in average. According to the SEM images, the prepared SAE–Fe_3O_4–NPs appeared in homogenous form, which confirms that the Fe_3O_4–NPs are cubic in shape with a slight difference in particle size that is ascribed to the presence of more faces in nano-crystallines due to its semi-uniform geometrical form (Sutradhar *et al.* 2011). Observation revealed that the crystalline structure of the prepared SAE–Fe_3O_4–NPs was supported by the correlation between the Scherrer equation and SEM particle sizes and that the morphology was predominantly porous and spongy (Uruş 2016). As observed in SEM images, the SAE–Fe_3O_4–NPs tend to aggregate, which may be attributed to the van der Waals force between particles. The agglomeration may be caused by the repulsive electrostatic forces between attracting particles closer to each other so they aggregate (Rosická & Šembera 2013).

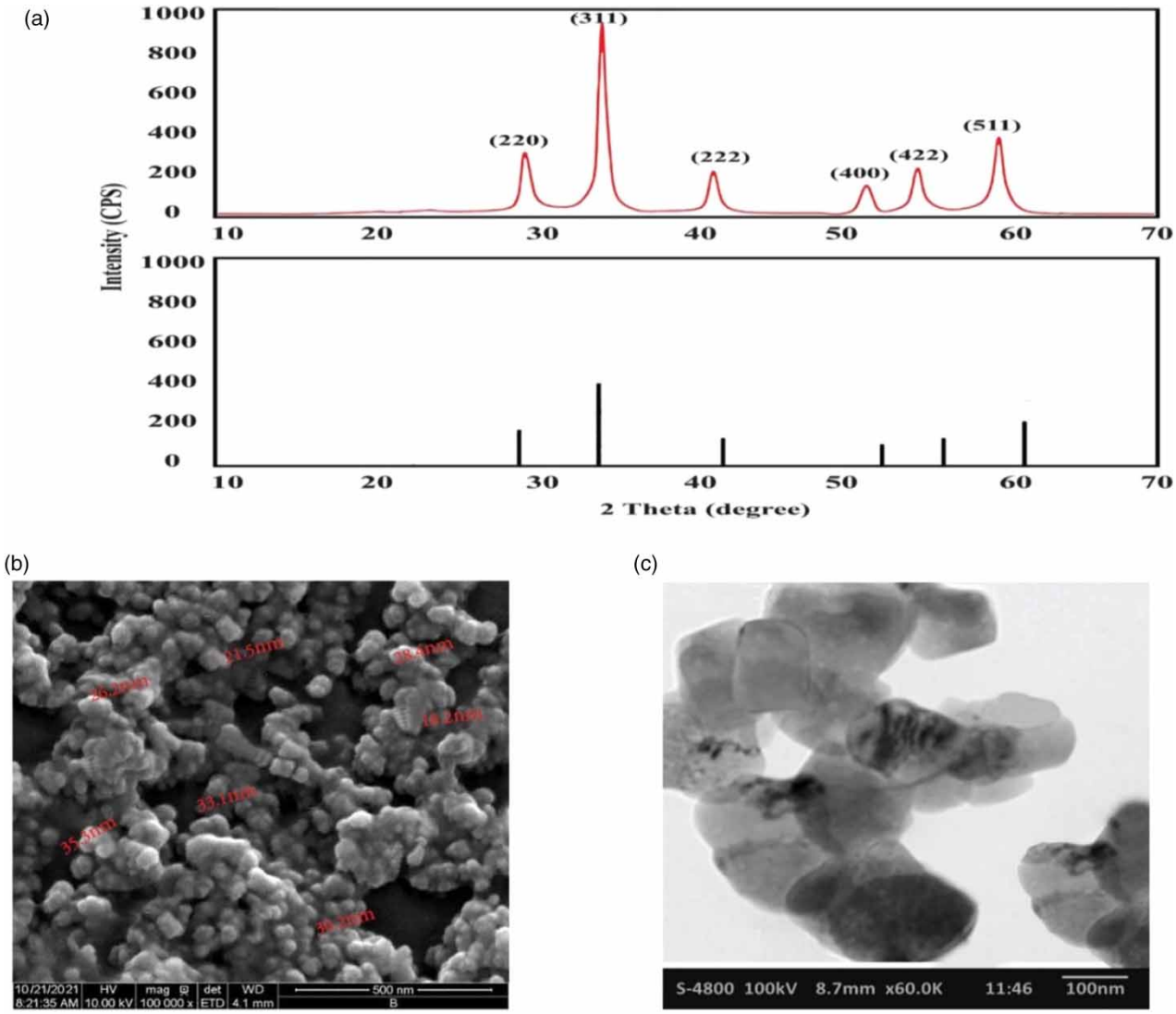

Figure 10 | Green biosynthesis of magnetite from SAE: (a) XRD patterns spectra, (b) SEM micrograph, and (c) TEM image.

Table 4 | Calculation of MNPS size using the Scherrer equation

Peak number	Pos. (2θ)	FWHM	Size (nm)
1	30.22	0.3825	21.72
2	35.60	0.3825	23.89
3	45.60	0.5510	23.99
4	54.10	0.4723	29.32
5	57.68	0.5723	31.44
6	63.10	0.6723	32.73

FWHM, full width at half maximum.

A drop of the green-synthesized MNPs by SAE was deposited onto a TEM copper grid for TEM. After drying, the grid was imaged using TEM at 100 kV. Figure 10(c) reveals the TEM image. It is evident from the TEM image that the sizes of MNP are almost homogeneous crystalline structures, and all of the particles are highly cubic in shape, slightly equal to or larger than

the calculated crystallite size from the XRD technique. Consequently, the XRD test can be used as a suitable method to evaluate the average size of crystallites; hence, the TEM technique can be appropriate for measuring particle size (Tamiji & Nezamzadeh-Ejhieh 2019).

3.7.3. The FTIR spectrum and absorption bands

FTIR analysis was done to define the functional groups of star anise that acted as bio-reduction of ferric chloride in the synthesis of MNPs. The FTIR spectrum of SAE is demonstrated in Figure 11(a). The spectra of the SAE revealed strong absorption bands at 3,312, 2,935, 1,614, 1,406, 1,255, 1,064, 800, 669, 600, and 547 cm^{-1} (Figure 11(a)), while the absorption bands of synthesized Fe_3O_4–NPs were observed at 3,402, 1,616, 680, 583 and 559 cm^{-1} (Figure 11(b)). FTIR analysis proved that the bio-reduction of ferric chloride into MNPs is due to the reduction by capping material of plant leaf extracts (Sulaiman *et al.* 2018). The strong absorption peak at 3,312 cm^{-1} in the SAE indicated the O–H stretching, proving the presence of alcohol and phenolic compounds or stretching of the –NH band of the amino group. In contrast, the presence peak at 2,935 cm^{-1} contributed to the C–H stretching vibrations of $–CH_3$ and $–CH_2$ functional groups (Awwad & Salem 2012). The absorption peaks at 1,614 and 1,406 cm^{-1} are due to the stretching vibration of C=C alkene and $–CH^3$ stretching, respectively, where the peaks belonging to 1,255 and 1,064 cm^{-1} corresponded to the asymmetric stretching vibration of the COO group. The peaks at 800, 669, and 600 cm^{-1} revealed the existence of an aromatic C–H bending band. Venkateswarlu *et al.* (2014) recorded that all the bands were shifted after green-synthesized nanoparticles, indicating the participation and interaction of nanoparticles with plant extract. FTIR spectrum of green-synthesized MNPs is presented in 9 b, disclosed peaks at 3,402 cm^{-1} corresponding to –OH stretching, indicating that OH stretching of the water in the precursor, which disappeared in the nanoparticles caused by the adsorbed water molecules. Since the nano-crystalline materials exhibit a high surface-to-volume ratio and thus absorb moisture (Lu *et al.* 2010), 1,616 cm^{-1} corresponds to C=O stretching vibration, confirming the presence of the ester group. The formation of MNPs is characterized by absorption bands from 650 to 446 cm^{-1}. This peak was absent in plant extract, indicating the formation of iron oxide nanoparticles, which aligns with the findings reported by Kumar Das *et al.* (2014).

3.8. Antibacterial effect comparisons

The antibacterial effect of green-biosynthesized MNPs using different concentrations from SAE (2.5, 5, and 10%) was determined by the disc diffusion method and was assessed by measuring IZDs around the discs, as shown in Table 5. Based on the results, SAE of 10% concentration was used in synthesizing MNPS revealed the highest antimicrobial activity against *A. denitrificans* OK560350, with IZDs reaching 25 mm, followed by *Y. enterocolitica* MZ673567 (20 mm IZDs), *S. marcescens* MZ618709 (17 mm IZDs), *S. flexneri* MZ350855 (17 mm IZDs), and *K. aerogenes* MZ352107 (15 mm IZDs) (Figure 12).

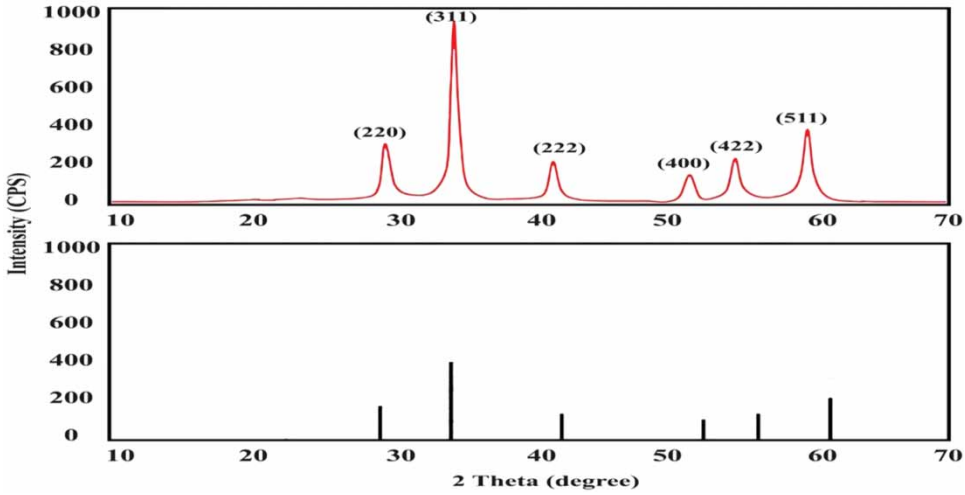

Figure 11 | FTIR analysis where (a) shows the spectrum of fruit SAE and (b) shows the spectrum of Fe_3O_4-MNPs synthesized by SAE.

Table 5 | Effect of different concentration percentages of SAE in biosynthesis of MNPs on isolated MAR bacteria

	IZD (mm)		
Bacterial isolates	**2.5%**	**5%**	**10%**
Shigella flexneri MZ350855	8 ± 0.85	12 ± 1.0	17 ± 1.0
Klebsiella aerogenes MZ352107	6 ± 1.0	11 ± 1.0	15 ± 0.87
Serratia marcescens MZ618709	6 ± 1.8	13 ± 0.85	17 ± 1.0
Yersinia enterocolitica MZ673567	8 ± 1.0	16 ± 1.0	20 ± 1.0
Achromobacter denitrificans OK560350	10 ± 1.0	17 ± 0.87	25 ± 1.0

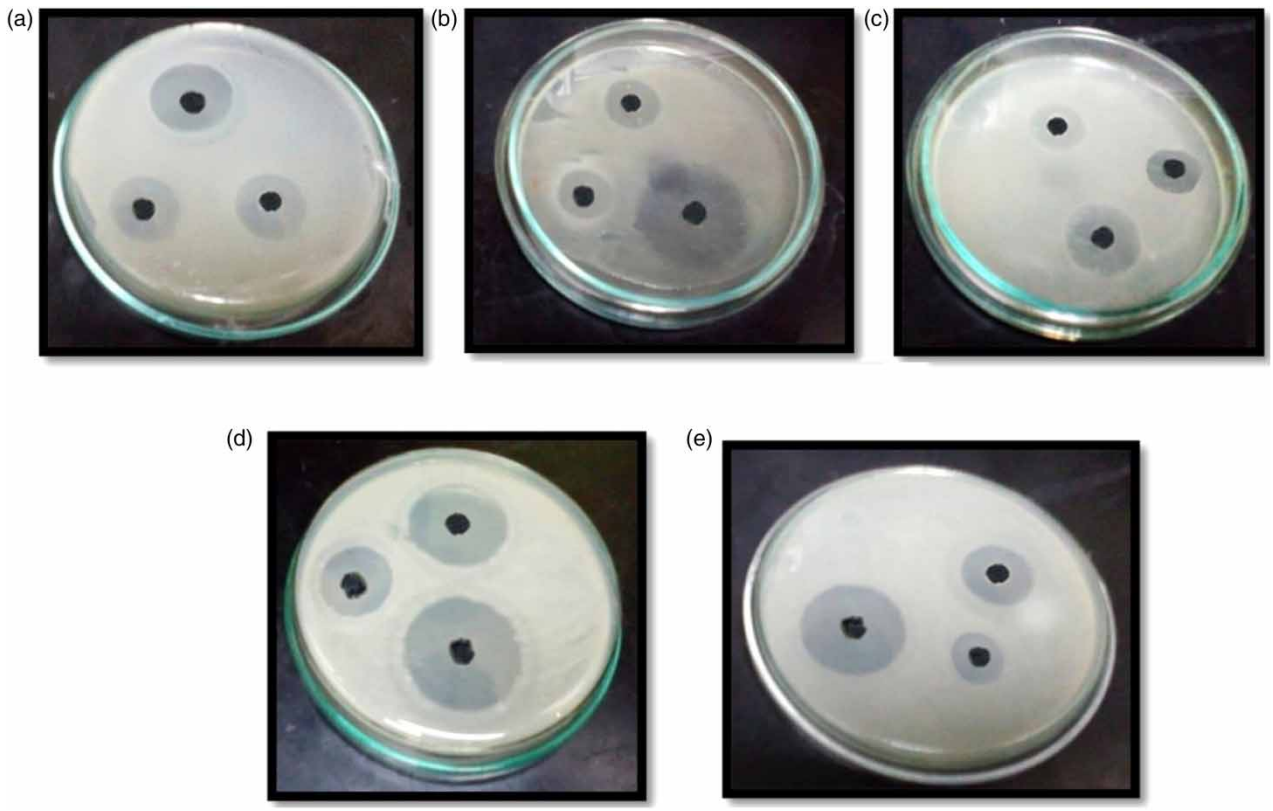

Figure 12 | Screening inhibition zones of different concentrations of SAE in green biosynthesis for magnetite using the agar disc diffusion method: (a) *Klebsiella aerogenes* MZ352107.1; (b) *Yersinia enterocolitica* MZ673567.1; (c) against *Serratia marcescens* MZ618709.1; (d) against *Achromobacter denitrificans* OK560350.1; and (e) against Shigella flexneri MZ350855.1.

3.9. Nanotechnology in wastewater treatment experiment

This study aimed to demonstrate the potential use of synthesized SAE–Fe_3O_4–NPs in the removal of contaminants from collected wastewater samples as applicable experiments. An overall schematic was set up, and employed results in the present study are shown in Table 6 and Figure 13. The antibacterial activity of biosynthesized magnetite by SAE was examined. The bacterial count was observed to be reduced to more than 20% in the treated flask with 0.01 g of SAE–Fe_3O_4–NPs compared with the wastewater sample that was not treated with any of the synthesized antibacterial agents. Based on the obtained CFU value and calculation from the percentage reduction of bacterial count in Equation (1), it is evident that the amount of bacteria colony in treated wastewater with synthesized MNPs was decreased by raising the added amounts of nanoparticles until reaching about 84% removal with 0.05 g of nanoparticles and appeared in Figure 13(c). From these observations, the antibacterial activity of SAE–Fe_3O_4–NPs against various types of water-borne bacteria was confirmed. Previous findings demonstrate

Table 6 | Water quality parameters of raw wastewater and treated water after the application of SAE–Fe_3O_4–NPs, and their removal efficiency (%)

			Treated water with SAE–Fe_3O_4–NPs									
Parameters	**Unites**	**Raw wastewater**	**0.01 g**	**%**	**0.02 g**	**%**	**0.03 g**	**%**	**0.04 g**	**%**	**0.05 g**	**%**
PH		7.29	7.19	–	7.10	–	7.11	–	7.20	–	7.30	–
Trace metal												
Al	mg/L	0.008	>0.001	87	>0.001	87	>0.001	87	>0.001	87	>0.001	87
Ba	mg/L	0.056	0.031	44	0.022	60	0.017	69	0.015	73	0.014	75
Cd	mg/L	2.404	1.081	55	0.983	59	0.040	98	0.016	99	0.013	99
Cu	mg/L	0.055	0.027	50	0.025	54	0.023	58	0.022	60	0.022	60
Fe	mg/L	0.655	0.320	51	0.101	84	0.005	99	>0.001	99	>0.001	99
Mo	mg/L	>0.001	>0.001	0	>0.001	0	>0.001	0	>0.001	0	>0.001	0
Pb	mg/L	3.021	2.001	33	1.043	65	0.026	99	0.019	99	0.017	99
Se	mg/L	>0.001	>0.001	0	>0.001	0	>0.001	0	>0.001	0	>0.001	0
Mn	mg/L	0.240	0.230	4	0.121	49	0.065	72	0.013	94	0.010	95
V	mg/L	0.011	0.011	0	0.011	0	0.011	0	0.011	0	0.011	0
Sn	mg/L	> 0.004	>0.004	0	>0.004	0	>0.004	0	>0.004	0	>0.004	0
Organic parameters												
BOD	mg/L	90.00	70	22	50	44	20	77	11	87	10	88
COD	mg/L	857.0	600	29	500	41	200	76	190	77	140	83
Microbiological parameters (count $\times 10^5$)												
Total bacterial count at 37 °C	(CFU/mL)	1,200	799	33	500	58	200	83	180	85	150	87
Total bacterial count at 22 °C	(CFU/mL)	2,250	1,800	20	800	64	600	73	400	82	350	84

that synthesized MNPs from pollen ethanolic extracts (PEEs) showed antimicrobial activity against a large antimicrobial spectrum, including Gram-positive, Gram-negative, and antifungal microorganisms (Spulber *et al.* 2018).

The control and treated flasks were examined for trace heavy metal (HMs) as an experiment to discuss the adsorption efficiency of SAE–Fe_3O_4–NPs. Some trace elements were determined and some of those elements below method detection limits (MDL) of ICP-OES instrument that used in analysis and standard limits of the Egyptian law EGL (92/2013) for wastewater. The trace elements were Mo (>0.001), Se (>0.001), ST (>0.005) and Sn (>0.004). The recorded value of Al, Ba, Cu, Fe and Mn were within the permissible value of EGL (92 /2013) limits for drain water. Therefore, the values of Cd and Pb were higher the permissible value of EGL (92/2013). After standing MNPs in the treated flask, they were collected magnetically. The concentration of the remaining metal ions was determined by the ICP-OES with USN, where this nebulizer decreases the instrument's detection limit by 10%. It was found that the removal percentage of the Pb^{2+}, Cd^{2+}, Fe^{2+} ions reach 99% after 30 min of the sample treatment, as depicted in Table 6. Recently, MNPs have received attention due to their high surface area and superior magnetic properties as an emerging adsorbent. Magnetite efficiency was investigated as adsorbents for Cd^{2+}, Pb^{2+}, and Zn^{2+} from wastewater (Yong-Gang *et al.* 2019). In water treatment methods using nano-sorbent materials, separating nanoparticles from contaminated water is challenging due to its small size. However, MNPs can be easily separated and recovered from the system by an external magnetic field. The removal percent of HMs can be calculated from Equation (3).

$$\text{Removal efficiency } \% = \frac{Vo - Ve}{Vo} \times 100 \tag{3}$$

where V_o is the initial volume of the heavy metal and V_e is the final volume of the heavy metal.

The values of biochemical oxygen demand (BOD) and chemical oxygen demand (COD) concentration reach high levels because of direct discharge of factories in qusena on El Khadrawia drain; the results exceed the permissible value of EGL

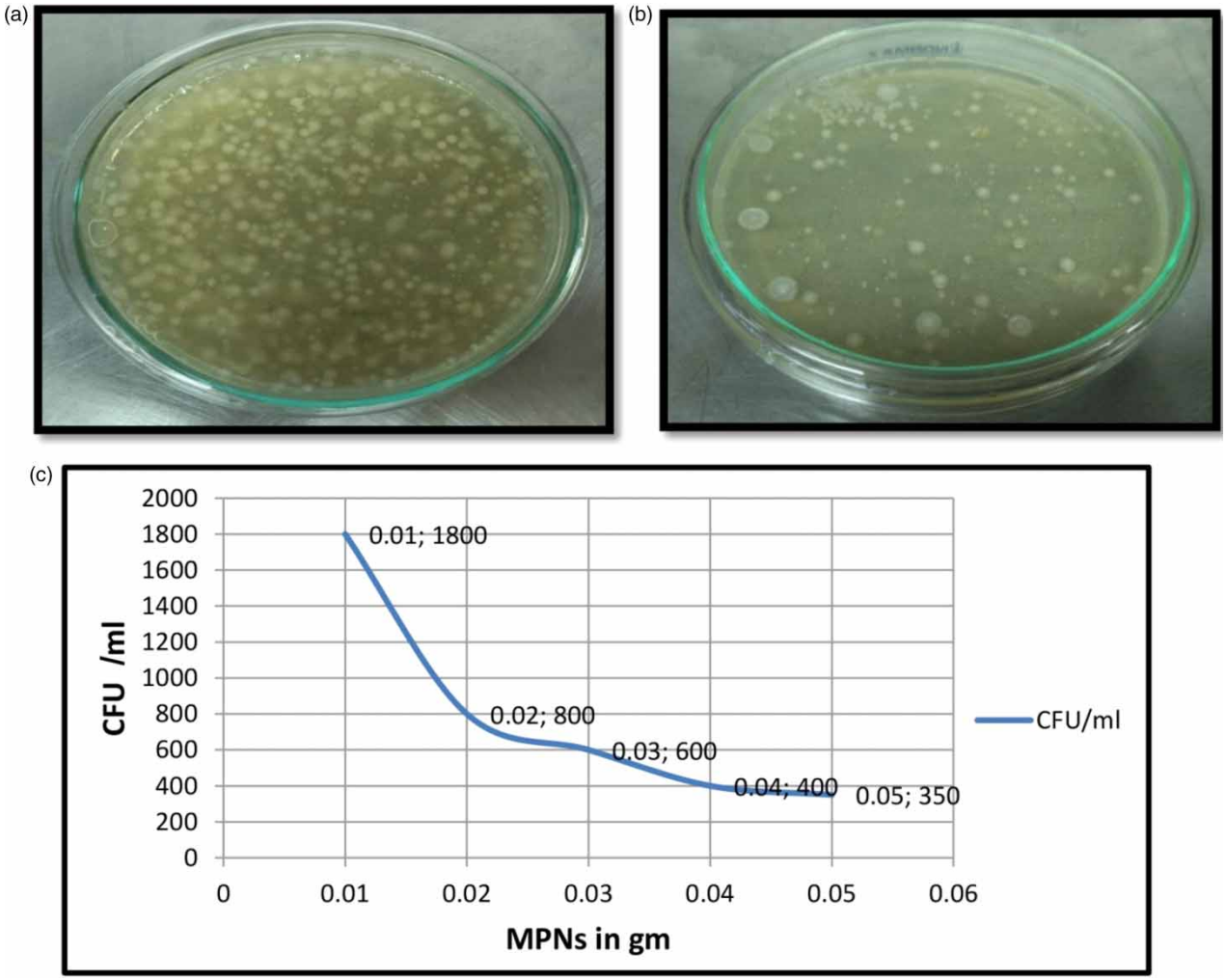

Figure 13 | Images of bacterial cultures of (a) untreated sample; (b) treated sample with MNPs by SAE; (c) bacterial concentration with respect to the amount of added MNPs.

(92 /2013). A notable decrease in BOD and COD values was observed after using SAE–Fe_3O_4–NPs in treatment with 88 and 83%, respectively, as presented in Table 6.

4. CONCLUSIONS

Several researchers are currently focusing on biomimetic approaches, such as plant extracts and microorganisms, to synthesize the nanoparticles, a 'green chemical or phytochemical' approach. Based on the current study findings, it can be concluded the ability for successful green syntheses of iron oxide magnetic nanoparticles by SAE and its effectiveness in decreasing the microbial content in wastewater samples as well as toxic metal adsorptive. The study also revealed that increasing the concentration of SAE resulted in increased inhibition activity against some isolated MAR bacteria from wastewater samples. In addition, an active compound named trans-1-methoxy-4-[prop-1-enil] benzene (anethole) was identified from SAE by GCMS analysis of partially purified SAE at a Rf value of 0.9, which was detected by thin-layer chromatography which has an antimicrobial effect and was promising in reducing MAR bacteria and may be help in the progress of new safe bactericidal products having a natural base. The heavy metal removal results show that the synthesized MNPs appear to be very promising material for wastewater treatment application. Therefore, SAE–Fe_3O_4–NPs offer promise for environment-friendly components for successful water treatment and thus will lead to an increase in safe water resources. Future application of a study to treat wastewater using green-synthesized magnetite for agriculture sector in water-scarce regions is recommended.

AUTHOR CONTRIBUTIONS

M.E.-S. provided conception and design of research; acquisition, analysis, and interpretation of data; drafted the manuscript and substantively revised it. S.A.O. processed creation of new software used in the research and revised the manuscript. All the authors read and approved the final manuscript.

AVAILABILITY OF DATA AND MATERIALS

All data analyzed during our study are from our own work and it is our pleasure to be available publically.

DATA AVAILABILITY STATEMENT

All relevant data are included in the paper or its Supplementary Information.

CONFLICT OF INTEREST

The authors declare there is no conflict.

REFERENCES

Aly, S. E., Sabry, B. A., Shaheen, M. S. & Hathout, A. S. 2016 Assessment of antimycotoxigenic and antioxidant activity of star anise (Illicium verum) in vitro. *Journal of the Saudi Society of Agricultural Sciences* **15** (1), 20–27.

American Public Health Association (APHA), American Water Works Association, Water Pollution Control Federation, & Water Environment Federation 2017 *Standard Methods for the Examination of Water and Wastewater*, Vol. 2. American Public Health Association, Washington, DC, USA.

Awwad, A. M. & Salem, N. M. 2012 A green and facile approach for synthesis of magnetite nanoparticles. *Nanoscience and Nanotechnology* **2** (6), 208–213.

Basavegowda, N., Magar, K. B. S., Mishra, K. & Lee, Y. R. 2014a Green fabrication of ferromagnetic Fe_3O_4 nanoparticles and their novel catalytic applications for the synthesis of biologically interesting benzoxazinone and benzthioxazinone derivatives. *New Journal of Chemistry* **38** (11), 5415–5420.

Basavegowda, N., Mishra, K. & Lee, Y. R. 2014b Sonochemically synthesized ferromagnetic Fe 3 O 4 nanoparticles as a recyclable catalyst for the preparation of pyrrolo [3, 4-c] quinoline-1, 3-dione derivatives. *RSC Advances* **4** (106), 61660–61666.

Bauer, A. W. 1966 Antibiotic susceptibility testing by a standardized single disc method. *American Journal of Clinical Pathology* **45**, 149–158.

César de Souza Vasconcelos, L., Sampaio, M. C. C., Sampaio, F. C. & Higino, J. S. 2003 Use of Punica granatum as an antifungal agent against candidosis associated with denture stomatitis. *Mycoses* **46** (5-6), 192–196.

Chen, D., Love, K. T., Chen, Y., Eltoukhy, A. A., Kastrup, C., Sahay, G. & Anderson, D. G. 2012 Rapid discovery of potent siRNA-containing lipid nanoparticles enabled by controlled microfluidic formulation. *Journal of the American Chemical Society* **134** (16), 6948–6951.

Clinical and Laboratory Standards Institute 2019 *Performance Standards for Antimicrobial Susceptibility Testing*, 29th edn. Washington, DC, USA. CLSI document, p. M100.

Demchenko, V., Riabov, S., Sinelnikov, S., Radchenko, O., Kobylinskyi, S. & Rybalchenko, N. 2020 Novel approach to synthesis of ssilver nanoparticles in interpolyelectrolyte complexes based on pectin, chitosan, starch and their derivatives complexes based on pectin, chitosan, starch and their derivatives. *Carbohydrate Polymers* **242**, 116431

Devatkal, S. K., Jaiswal, P., Jha, S. N., Bharadwaj, R. & Viswas, K. N. 2013 Antibacterial activity of aqueous extract of pomegranate peel against Pseudomonas stutzeri isolated from poultry meat. *Journal of Food Science and Technology* **50** (3), 555–560.

Dipankar, C. & Murugan, S. 2012 The green synthesis, characterization and evaluation of the biological activities of silver nanoparticles synthesized from Iresine herbstii leaf aqueous extracts. *Colloids and Surfaces B: Biointerfaces* **98**, 112–119.

Dorman, H. D. & Deans, S. G. 2000 Antimicrobial agents from plants: antibacterial activity of plant volatile oils. *Journal of Applied Microbiology* **88** (2), 308–316.

Etemadifar, R., Kianvash, A., Arsalani, N., Abouzari-Lotf, E. & Hajalilou, A. 2018 Green synthesis of superparamagnetic magnetite nanoparticles: effect of natural surfactant and heat treatment on the magnetic properties. *Journal of Materials Science: Materials in Electronics* **29** (20), 17144–17153.

Fauzi, N. N., Hamdan, R. H., Mohamed, M., Ismail, A., Zin, A. A. & Mohamad, N. F. 2021 Prevalence, antibiotic susceptibility, and presence of drug resistance genes in Aeromonas spp. isolated from freshwater fish in Kelantan and Terengganu states, Malaysia. *Veterinary World* **14** (8), 2064.

Giraldo, L., Erto, A. & Moreno-Piraján, J. C. 2013 Magnetite nanoparticles for removal of heavy metals from aqueous solutions: synthesis and characterization. *Adsorption* **19** (2), 465–474.

Handayani, W., Ningrum, A. S. & Imawan, C. 2020 The role of pH in synthesis silver nanoparticles using Pometia pinnata (Matoa) leaves extract as bioreductor. *Journal of Physics: Conference Series* **1428** (1), 1–5.

Holt, J. C. & Krieg, N. R. 1984 *Bergeys' Manual of Systemic Bacteriology*, Vol. 9, 4th edn. William and Wilkins, Baltimore, MD, USA, pp. 40–97.

Houston, D. M., Bugert, J. J., Denyer, S. P. & Heard, C. M. 2017 Potentiated virucidal activity of pomegranate rind extract (PRE) and punicalagin against Herpes simplex virus (HSV) when co-administered with zinc (II) ions, and antiviral activity of PRE against HSV and aciclovir-resistant HSV. *PloS One* **12** (6), e0179291.

Ismail, M., Essam, T., Mohamed, A. & Mourad, F. 2012 Screening for the antimicrobial activities of alcoholic and aqueous extracts of some common spices in Egypt. *Microbiological Research* **3**, 200–207.

Iversen, A., Kühn, I., Rahman, M., Franklin, A., Burman, L. G., Olsson-Liljequist, B., Torell, E. & Möllby, R. 2004 Evidence for transmission between humans and the environment of a nosocomial strain of Enterococcus faecium. *Environmental Microbiology* **6** (1), 55–59.

Ize-Ludlow, D., Ragone, S., Bruck, I. S., Bernstein, J. N., Duchowny, M. & Peña, B. M. G. 2004 Neurotoxicities in infants seen with the consumption of Star anise tea. *Pediatrics* **114** (5), e653–e656.

Kessie, G., Ettayebi, M., Haddad, A. M., Shibl, A. M., Al-Shammary, F. J., Tawfik, A. F. & Al-Ahdal, M. N. 1998 Plasmid profile and antibiotic resistance in coagulase-negative staphylococci isolated from polluted water. *Journal of Applied Microbiology* **84** (3), 417–422.

Kim, Y., Lee Chung, B., Ma, M., Mulder, W. J., Fayad, Z. A., Farokhzad, O. C. & Langer, R. 2012 Mass production and size control of lipid–polymer hybrid nanoparticles through controlled microvortices. *Nano Letters* **12** (7), 3587–3591

Klnight, V., Sanglier, J. J., DiTullio, D., Braccili, S., Bonner, P., Waters, J., Hughes, D. & Zhang, L. 2003 Diversifying microbial natural products for drug discovery. *Applied Microbiology and Biotechnology* **62** (5), 446–458.

Kloy, A., Ahmad, J., Yusuf, U. & Muhammad, M. 2020 Antibacterial properties of rosemary (Rosmarinus officinalis). *South. Asian. Res. J. Pharm. Sci* **2** (1), 4–7.

Kumar Das, A., Marwal, A. & Verma, R. 2014 Bio-reductive synthesis and characterization of plant protein coated magnetite nanoparticles. *Nano Hybrids* **7** (2), 69–86.

Lu, W., Shen, Y., Xie, A. & Zhang, W. 2010 Green synthesis and characterization of superparamagnetic Fe_3O_4 nanoparticles. *Journal of Magnetism and Magnetic Materials* **322** (13), 1828–1833.

Mahdavi, M., Namvar, F., Ahmad, M. B. & Mohamad, R. 2013 Green biosynthesis and characterization of magnetic iron oxide (Fe_3O_4) nanoparticles using seaweed (Sargassum muticum) aqueous extract. *Molecules* **18** (5), 5954–5964.

Marinov, V. & Valcheva-Kuzmanova, S. 2015 Review on the pharmacological activities of anethole. *Scripta Scientifica Pharmaceutica* **2** (2), 14–19.

Marquez, C. A., Wang, H., Fabbretti, F. & Metzger, J. O. 2008 Electron-transfer-catalyzed dimerization of trans-anethole: detection of the distonic tetramethylene radical cation intermediate by extractive electrospray ionization mass spectrometry. *Journal of the American Chemical Society* **130** (51), 17208–17209.

Megha, V., Meenakshi, S. & Rai, J. P. N. 2015 Optimization of different parameters on synthetic dye decolorization by free and immobilized Mucor hiemalis MV04 (KR078215). *Research Journal of Chemical Sciences* **5** (6), 20–27.

Moniruzzaman, M., Shahinuzzaman, M., Haque, A., Khatun, R. & Yaakob, Z. 2015 Gas chromatography mass spectrometry analysis and in vitro antibacterial activity of essential oil from Trigonella foenum-graecum. *Asian Pacific Journal of Tropical Biomedicine* **5**, 1033–1036.

Muralikrishna, T., Pattanayak, M. & Nayak, P. L. 2014 Green synthesis of gold nanoparticles using (aloe vera) aqueous extract. *World Journal of Nano Science & Technology* **3** (2), 45–51.

Najdoska, M., Bogdanov, J. & Zdravkovski, Z. 2010 TLC and GC-MS analyses of essential oil isolated from Macedonian Foeniculi fructus. *Macedonian Pharmaceutical Bulletin* **56** (1), 2.

Narayanan, S., Sathy, B. N., Mony, U., Koyakutty, M., Nair, S. V. & Menon, D. 2012 Biocompatible magnetite/gold nanohybrid contrast agents via green chemistry for MRI and CT bioimaging. *ACS Applied Materials & Interfaces* **4** (1), 251–260.

Njagi, E. C., Huang, H., Stafford, L., Genuino, H., Galindo, H. M., Collins, J. B., Hoag, G. E. & Suib, S. L. 2011 Biosynthesis of iron and silver nanoparticles at room temperature using aqueous sorghum bran extracts. *Langmuir* **27** (1), 264–271.

Noginov, M. A., Zhu, G., Bahoura, M., Adegoke, J., Small, C., Ritzo, B. A., Drachev, V. P. & Shalaev, V. M. 2007 The effect of gain and absorption on surface plasmons in metal nanoparticles. *Applied Physics B* **86** (3), 455–460.

Pinto, R. J., Neves, M. C., Neto, C. P. & Trindade, T. 2012 Composites of cellulose and metal nanoparticles. *Nanocomposites–New Trends and Developments* **2** (3), 1–25.

Prakash, D., Ramesh, K., Gopinath, N., Shantha Kumar, S. S. & Varuvelil, G. J. 2014 Antibacterial efficacy of Syzygium aromaticum extracts on multi-drug resistant streptococcus mutans isolated from dental plaque samples. *Journal of Biochemical Technology* **3** (5), 155–157.

Priyadarsini, S., Mukherjee, S., Bag, J., Nayak, N. & Mishra, M. 2020 Application of nanoparticles in dentistry: current trends. In: Shukla, A. (ed.) *Nanoparticles in Medicine*. Springer, Singapore, pp. 55–98.

Qiao, H., Meifang, Z. & Shuyong, W. 2018 Progress on the antimicrobial activity research of clove oil and eugenol in the food antisepsis field. *Journal of Food Science* **83**, 1476–1483.

Rengga, W. D. P., Yufitasari, A. & Adi, W. 2017 Synthesis of silver nanoparticles from silver nitrate solution using green tea extract (Camelia sinensis) as bioreductor. *JBAT* **6** (1), 32–38.

Rosická, D. & Šembera, J. 2013 Changes in the nanoparticle aggregation rate due to the additional effect of electrostatic and magnetic forces on mass transport coefficients. *Nanoscale Research Letters* **8** (1), 1–9.

Santos, T., Silva, N., Igrejas, G., Rodrigues, P., Micael, J., Rodrigues, T., Resendes, R., Gonçalves, A., Marinho, C., Gonçalves, D., Cunha, R. & Poeta, P. 2013 Dissemination of antibiotic resistant Enterococcus spp. and Escherichia coli from wild birds of Azores Archipelago. *Anaerobe* **24**, 25–31.

Sarg, T. M., Salem, S. A., Farrag, N. M., Abdel-Aal, M. M. & Ateya, A. M. 1990 Phytochemical and antimicrobial investigation of Hemerocallis fulva L. grown in Egypt + . *International Journal of Crude Drug Research* **28** (2), 153–156.

Savage, N. & Diallo, M. S. 2005 Nanomaterials and water purification: opportunities and challenges. *Journal of Nanoparticle Research* **7** (4), 331–342.

Sawatzky, P., Liu, G., Dillon, J. A. R., Allen, V., Lefebvre, B., Hoang, L., Tyrrell, G., Van Caeseele, P., Levett, P. & Martin, I. 2015 Quality assurance for antimicrobial susceptibility testing of Neisseria gonorrhoeae in Canada, 2003 to 2012. *Journal of Clinical Microbiology* **53** (11), 3646–3649.

Senthil, M. & Ramesh, C. 2012 Biogenic synthesis of Fe_3O_4 nanoparticles using tridax procumbens leaf extract and its antibacterial on Pseudomonas Aeruginosa. *Digest Journal of Nanomaterials & Biostructures (DJNB)* **7** (4), 212–230 .

Sneath, P. H. A. 1986 Estimating uncertainty in evolutionary trees from Manhattan-distance triads. *Systematic Zoology* **35** (4), 470–488.

Sonibare, M. A., Ayoola, I. O. & Elufioye, T. O. 2017 Antioxidant and acetylcholinesterase inhibitory activities of leaf extract and fractions of Albizia adianthifolia (Schumach) WF wright. *Journal of Basic and Clinical Physiology and Pharmacology* **28** (2), 143–148.

Spulber, R., Chifiriuc, C., Fleancu, M., Popa, O. & Băbeanu, N. 2018 Antibacterial activity of magnetite nanoparticles coated with bee pollen extracts. In *Agriculture for Life, Life for Agriculture' Conference Proceedings*, pp. 579–585.

Sri, P. U., Leelavathi, V., Sree, N. V. & Kumar, M. A. 2015 Antihelmenthic and antimicrobial activity of green synthesized silver nanoparticles from Illicium Verum Hook. F. Fruit. *IOSR Journal of Pharmacy and Biological Sciences* **10** (6), 61–65.

Sulaiman, G. M., Tawfeeq, A. T. & Naji, A. S. 2018 Biosynthesis, characterization of magnetic iron oxide nanoparticles and evaluations of the cytotoxicity and DNA damage of human breast carcinoma cell lines. *Artificial Cells, Nanomedicine, and Biotechnology* **46** (6), 1215–1229.

Sutradhar, N., Sinhamahapatra, A., Pahari, S. K., Pal, P., Bajaj, H. C., Mukhopadhyay, I. & Panda, A. B. 2011 Controlled synthesis of different morphologies of MgO and their use as solid base catalysts. *The Journal of Physical Chemistry C* **115** (25), 12308–12316.

Tadesse, Z., Kelbessa, E. & Bekele, T. 2017 Floristic composition and plant community analysis of vegetation in Ilu Gelan district, West Shewa Zone of Oromia region, Central Ethiopia. *Tropical Plant Research* **4** (2), 335–350.

Tamiji, T. & Nezamzadeh-Ejhieh, A. 2019 Study of kinetics aspects of the electrocatalytic oxidation of benzyl alcohol in aqueous solution on AgBr modified carbon paste electrode. *Materials Chemistry and Physics* **237**, 121813.

Uruş, S. 2016 Synthesis of Fe_3O_4- SiO2- OSi (CH2) 3NHRN (CH2PPh2) 2pdcl2 type nanocomposite complexes: highly efficient and magnetically-recoverable catalysts in vitamin K3 synthesis. *Food Chemistry* **213**, 336–343.

Venkateswarlu, S., Rao, Y. S., Balaji, T., Prathima, B. & Jyothi, N. V. V. 2013 Biogenic synthesis of Fe_3O_4 magnetic nanoparticles using plantain peel extract. *Materials Letters* **100**, 241–244.

Venkateswarlu, S., Kumar, B. N., Prasad, C. H., Venkateswarlu, P. & Jyothi, N. V. V. 2014 Bio-inspired green synthesis of Fe_3O_4 spherical magnetic nanoparticles using Syzygium cumini seed extract. *Physica B: Condensed Matter* **449**, 67–71.

Wang, G. W., Hu, W. T., Huang, B. K. & Qin, L. P. 2011 Illicium verum: a review on its botany, traditional use, chemistry and pharmacology. *Journal of Ethnopharmacology* **136** (1), 10–20.

World Health Organization 2014 *Antimicrobial Resistance Global Report on Surveillance: 2014 Summary (No. WHO/HSE/PED/AIP/2014.2)*. World Health Organization, Geneva, Switzerland.

Yong-Gang, S. U. I., Si-Yong, T. E. N. G., Jie, Q. I. A. N., Yuan, W. U., Ke-Fei, D. O. U., Yi-Da, T. A. N. G. & Yong-Jian, W. U. 2019 Invasive versus conservative strategy in consecutive patients aged 80 years or older with non-ST-segment elevation myocardial infarction: a retrospective study in China. *Journal of Geriatric Cardiology* **16** (10), 741–748.

First received 20 October 2022; accepted in revised form 9 January 2023. Available online 20 January 2023